

# Forces between functionalized silica nanoparticles in solution

J. Matthew D. Lane,<sup>1</sup> Ahmed E. Ismail,<sup>1</sup> Michael Chandross,<sup>1</sup> Christian D. Lorenz,<sup>2</sup> and Gary S. Grest<sup>1</sup>

<sup>1</sup>*Sandia National Laboratories, Albuquerque, NM 87185*

<sup>2</sup>*Materials Research Group, King's College, London, WC2R 2LS, UK*

(Dated: April 12, 2022)

To prevent the flocculation and phase separation of nanoparticles in solution, nanoparticles are often functionalized with short chain surfactants. Here we present fully-atomistic molecular dynamics simulations which characterize how these functional coatings affect the interactions between nanoparticles and with the surrounding solvent. For 5 nm diameter silica nanoparticles coated with poly(ethylene oxide) (PEO) oligomers in water, we determined the hydrodynamic drag on two approaching nanoparticles moving through solvent and on a single nanoparticle as it approaches a planar surface. In most circumstances, macroscale fluid theory accurately predicts the drag on these nano-scale particles. Good agreement is seen with Brenner's analytical solutions for wall separations larger than the soft nanoparticle radius. For two approaching coated nanoparticles, the solvent-mediated (velocity-independent) and lubrication (velocity-dependent) forces are purely repulsive and do not exhibit force oscillations that are typical of uncoated rigid spheres.

There is increasing interest in using nanoparticles in commercial and industrial applications. However, effective processing of nanoparticles requires that they do not aggregate and often involves solvation in a fluid. Functionalizing the nanoparticles accomplishes both goals. The behavior of functionalized nanoparticles depends strongly on the attached groups. The behavior of bare, nonfunctionalized nanoparticles has been studied via experiments, theory, and simulation, as have the interactions of polymer-grafted surfaces [1, 2, 3, 4]. The hydrodynamic and nanoparticle-nanoparticle interactions involving small functionalized nanoparticles, however, are harder to characterize. Experimentally, it is difficult to manipulate and measure forces on individual nanoparticles smaller than  $\sim 100$  nm. Theoretical treatments are challenging because the coatings are relatively short, while the particles themselves are outside the large radius of curvature limit. Numerical simulations of discrete solvent effects on nanoparticles have been impractical until now because of the large systems required to avoid significant finite-size effects due to the long-range hydrodynamic interactions. For single-particle diffusion, these corrections have been shown [5, 6] to scale as  $R/L$  where  $R$  is the particle radius and  $L$  is the simulation cell length.

Recent studies have computed the potential of mean force for bare silica nanoparticles in an aqueous medium, with and without electrolytes present [7]. Forces between bare colloidal nanoparticles have also been studied in Lennard-Jones fluids and in *n*-decane [8]. Hydrodynamic drag influenced by approach to a plane surface has been studied theoretically [9] and compared to simulations for rigid spheres [10, 11]. Alignment effects for amorphous nanoparticles have also been studied [12]. Kim *et al.* [13] used molecular dynamics (MD) simulations to study the relaxation of a fullerene molecule coated with poly(ethylene oxide) (PEO). Other simulations have either relied upon implicit solvents [14] or studied nanoparticles in a vacuum [15, 16].

An inherent feature of interacting functionalized nanoparticles in solution is the multiplicity of forces at both the atomistic and nanoparticle scales. At the atomistic scale these include electrostatic, van der Waals, bond, angle, and torsion forces. At the nanoparticle scale, these same forces can be assigned to hydrodynamic drag, lubrication, and depletion forces [17]. These latter forces are strongly dependent on the molecular structure of the nanoparticle coatings and solvent as well as the nanoparticle's velocity, size, and charge distribution.

In this Rapid Communication we present results of MD simulations of coated nanoparticles in an explicit solvent. We model the forces between atoms and directly measure the resulting forces on nanoparticles from their motion through the discrete fluid. To our knowledge, these are the first reported simulations of coated nanoparticle dynamics in an explicit, atomistic solvent. These and future results will allow for more accurate and efficient coarse-grained potentials which characterize the interactions of small functionalized nanoparticles in flow environments.

Two geometries are presented. First, a single functionalized nanoparticle approaching a fixed wall; and second, two nanoparticles approaching each other. We find good agreement with continuum theory in the first case even for these nanoscale particles. Comparison with the solved hydrodynamic problem of a rigid sphere approaching a wall [9] allows us to study system size effects. Static forces and velocity-dependent forces are reported.

We modeled 5 nm diameter rigid amorphous silica nanoparticles onto which a passivating coating of methyl-terminated PEO oligomer chains ( $\text{Si}(\text{OH})_3\text{CH}_2(\text{CH}_2\text{CH}_2\text{O})_6(\text{CH}_3)$ ) is attached. An example is shown in Figure 1. The chains were chemisorbed with trisilanol groups. The grafting density was 3.1 chains per  $\text{nm}^2$ , which gave approximately 240 chains per 5 nm nanoparticle. This density is consistent with experimental measurements [18]. We used all-atom force fields developed by Smith *et al.* for both the PEO [19] and the silica interactions [20]. We used the TIP4P water model [21]. While PEO-water interactions were explicitly provided, the silica-water interactions were determined by fitting the attractive portion of the Buckingham potentials to a Lennard-Jones potential and

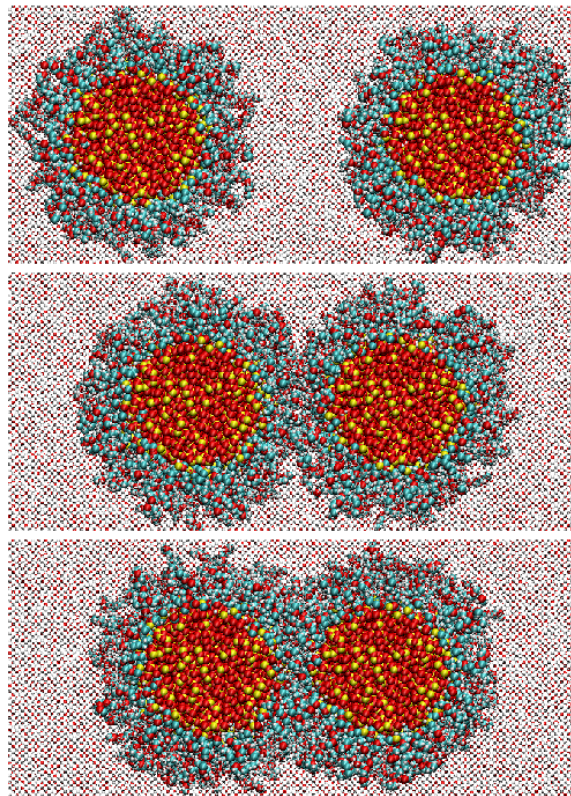


FIG. 1: (Color online) Cross sections of silica nanoparticles coated with PEO oligomers in water. Frames show a  $7\text{ nm} \times 15\text{ nm}$  view of the larger  $26\text{ nm} \times 26\text{ nm} \times 46\text{ nm}$  system. The nanoparticles are shown at center separations of 11.5 nm (top), 8.0 nm (middle), and 6.0 nm (bottom). Elements C, O, H, and Si are blue, red, white and yellow, respectively.

then combining them with the TIP4P potential using Lorentz-Berthelot mixing rules. Simulations were carried out using the LAMMPS classical MD code [22]. Numerical integration was performed using the velocity-Verlet algorithm with 1 fs timestep. Long-range Coulomb interactions were calculated using the PPPM method [23]. Unless otherwise stated, runs were made in the  $NVT$  ensemble with Nose-Hoover thermostat at 300 K with 100 fs damping time. Several were also run in the microcanonical ( $NVE$ ) ensemble to test the thermostat influence. As described below, no temperature drift was observed over the length of the  $NVE$  runs and the  $NVT$  and  $NVE$  ensembles give statistically identical results. However, the addition of a Langevin thermostat increased the drag force on the particles.

The nanoparticle cores were cut from bulk amorphous silica and then annealed to produce a surface OH concentration consistent with experimental values. The bulk silica was generated from a melt-quench process similar to the method of Lorenz *et al.* [24]. The nanoparticle core was treated as a rigid body. To build the composite systems containing water and a nanoparticle, we first equilibrated a large rectangular cell of TIP4P water at 300 K for 1 ns. The composite system, created by inserting the nanoparticle into a spherical hole cut in the periodic bulk solvent, was then equilibrated in an  $NPT$  ensemble at 300 K and 1 atm pressure for 0.5 ns. The viscosity of pure water at 1 atm was calculated using the Müller-Plathe [25] reverse perturbation method. The shear simulations were run on a  $13.0\text{ nm} \times 13.0\text{ nm} \times 11.5\text{ nm}$  shear cell simulation for more than 2 ns. The calculated viscosity of 0.55 cP is in agreement with previous simulations [26].

Three single-nanoparticle systems of varying sizes were built to determine any finite-size effects on the viscous drag. We varied  $L_{\perp} = L_x = L_y$  perpendicular to the direction of motion, while fixing  $L_z = 23.0\text{ nm}$ . For  $L_{\perp} = 13.0, 26.0$  and  $39.0\text{ nm}$  the systems contained approximately 400,000, 1.6 million and 3.6 million atoms, respectively. Systems with two nanoparticles were created by replicating the cell in the  $z$ -direction. These systems had dimensions  $L_{\perp} \times L_{\perp} \times 46.0\text{ nm}$ . For the largest simulations of more than 7 million atoms, 1 ns of simulation time took 140 hours on 1024 Intel Xeon processors.

We measured the forces on the nanoparticles as a function of separation for a nanoparticle approaching a plane surface and for the collision of two nanoparticles. In both scenarios, the nanoparticle core move at constant center-of-mass velocity, which was controlled by displacing the rigid silica core at a fixed rate while allowing rotation. The coating and solvent responded dynamically. Because the displacement of the nanoparticles was constrained, we were

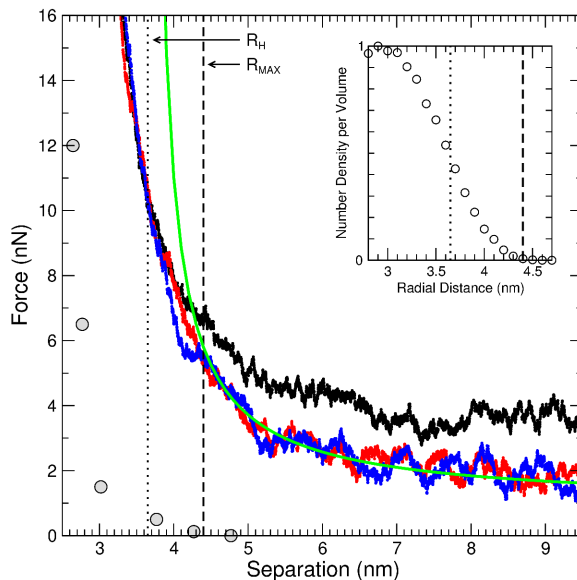


FIG. 2: (Color online) Force on nanoparticles approaching a plane surface of immobile water at 25 m/s as a function of center separation. The smallest system, with  $L_{\perp} = 13$  nm (black), shows a finite system size effect. The larger systems, with  $L_{\perp} = 26$  nm (red) and  $L_{\perp} = 39$  nm (blue), converge to the Brenner prediction (green) for separations greater than 4.4 nm. The open circles are equilibrated forces in which the particles are held fixed at a given separation.  $R_{\max}$  (dashed) and  $R_h$  (dotted) are defined in the text. Inset shows the time-averaged coating density versus radial distance.

able to measure the force response as a function of position for several approach velocities. The force on a nanoparticle core was computed by summing all individual forces acting on all atoms within the core. Forces were calculated every time step and averaged over 10 ps periods to remove atom-scale fluctuations.

**Nanoparticle approaching a plane surface** — The increased drag due to solvent-mediated interaction on a single spherical particle approaching a wall was derived analytically by Brenner [9]. Stokes drag, valid in the asymptotic limit far from the wall, is modified by a multiplicative correction,  $F_{\text{drag}} = 6\pi\mu Rv\lambda$ , where

$$\lambda = \frac{4}{3} (\sinh \alpha) \sum_{n=1}^{\infty} \frac{n(n+1)}{(2n-1)(2n+3)} \times \left[ \frac{2 \sinh((2n+1)\alpha) + (2n+1) \sinh 2\alpha}{4 \sinh^2((n+\frac{1}{2})\alpha) - (2n+1)^2 \sinh^2 \alpha} - 1 \right],$$

$\alpha = \cosh^{-1}(h/R)$ ,  $\mu$  is the solvent bulk viscosity,  $R$  is the radius,  $v$  is the sphere velocity, and  $h$  is the distance to the wall.

Recent explicit solvent simulations of rigid nanoparticles [11] have shown force oscillations near rigid walls. We find no oscillations for coated nanoparticles, while for bare silica nanoparticles we did observe oscillations.

Figure 2 shows the force on a PEO coated silica nanoparticle moving at 25 m/s as it approaches a wall of immobile water at the system boundary for three system sizes. This simple wall was selected to provide a hydrodynamic obstacle without altering the long-range coulombic interactions of the periodic cell, or introducing an effective wall potential. Two average radii are plotted as vertical lines:  $R_{\max} = 4.4$  nm is the radius at which the particle density of the coating falls to zero, and  $R_h = 3.65$  nm is the radius at which the particle density of the coating drops to half-maximum value.  $R_h$  is used for the effective hydrodynamic radius in subsequent drag calculations. The systems have maximum Reynolds number 0.33, indicating laminar flow and Schmidt number 180, indicating a momentum transfer dominated regime.

Using multiple system sizes allows us to determine the finite system-size effects on the measured forces. For separations greater than  $R_{\max}$ , finite system-size effects are evident in the smallest system. Results for the two larger systems show no system-size dependence and appear to have converged to the Brenner result. The observed forces depart from the Brenner solution for distances less than  $R_{\max}$ . The coating compresses on the surface to produce a softer force response than Brenner predicts for a hard sphere. At these separations, short-range contact forces rather than hydrodynamic forces dominate the nanoparticle interaction. Water molecules become trapped in the chains rather than flowing out of the gap. Moreover, the direct van der Waal and Coulomb interactions between particle

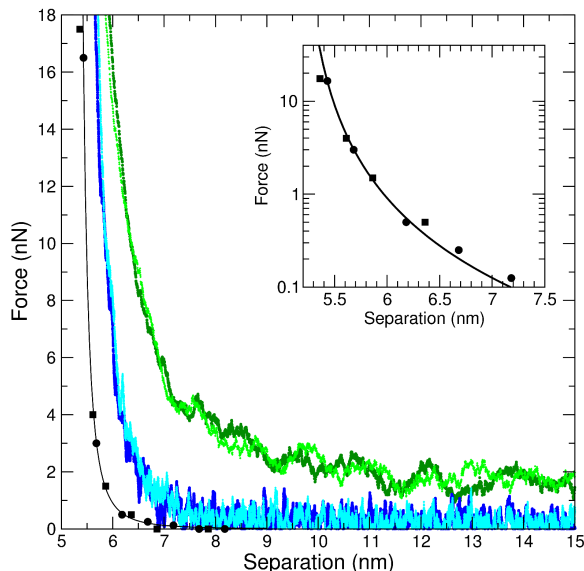


FIG. 3: (color online) Force on approaching nanoparticles with relative velocities of 5 m/s (light blue and dark blue) and 50 m/s (light green and dark green) as a function of center separation. The lighter colors are data from runs in the NVE ensemble and the darker colors were run in the thermostated NVT ensemble. Data for equilibrated configurations are shown in black. Inset shows the equilibrated data as a log-linear plot. Circles and squares are for  $L_{\perp}$  of 13 nm and 26 nm, respectively.

coating and wall becomes significant. Nanoparticles in all three system sizes feel identical forces for separations less than  $R_h$  at a given velocity. For separations greater than  $R_{\max}$ , the lubrication forces are strongly dependent on system size for small systems ( $L/R \sim 3$ ), but fall away rapidly with increase system size. This perhaps indicates that the short-range hydrodynamics dominate over long-range hydrodynamics which are predicted to fall away much more slowly, scaling as  $R/L$  [5, 6].

**Force between two nanoparticles** — The cross sections in Fig. 1 depict the system we used to study the forces between two nanoparticles. The two-nanoparticle dynamic simulations were run with system size  $L_{\perp} = 26$  nm and  $L_z = 46$  nm. Equilibration runs for smaller  $L_{\perp} = 13$  nm and  $L_z = 23$  nm systems are also reported. As seen in Fig. 1, the chains begin to touch when the center separation is approximately 8.5 nm. At 6.0 nm, the tethered chains are highly compressed.

Relative velocities of 5 and 50 m/s were used to determine the velocity-dependent lubrication forces. Starting at a core-core separation of 23 nm the nanoparticles were brought together until the forces between the two nanoparticles diverged. For the velocity independent solvation forces, the cores were held at various fixed positions taken from the finite velocity approach runs and each allowed to relax for 2 ns.

Figure 3 shows the force measured as a function of separation. The NVT and NVE ensembles give statistically identical results. The force is purely repulsive and, although fluctuating, on average increases monotonically with decreasing separation. The force response is consistent with the theoretical linear scaling in velocity and goes asymptotically to the single-particle Stokes drag in the limit of large separation. As in the single-particle study, we do not observe oscillations in the force which have been observed with two rigid sphere nanoparticles in explicit solvent [12].

Finite-system effects are expected for small systems at higher velocities. However, the equilibrated solvation forces showed no system size effects even for the smallest systems. The inset in figure 3 shows equilibrated forces computed in  $L_{\perp} = 13$  nm and 26 nm systems. The equilibrated force is plotted at fixed separations and fit within this range of separation by  $F_{\text{equil}} \propto (1/r)^{2.5}$ , where  $r$  is the core surface separation.

The two-nanoparticle data can be broken into three regimes, which we will refer to as large separations (greater than 8 nm), moderate separations (between 6 and 8 nm), and very small separations (less than 6 nm). These regimes are characterized by nanoparticle-nanoparticle forces which are non-interacting, weakly interacting, and strongly interacting, respectively. At large separations, the force on the nanoparticles is dominated by a constant resistance to motion by the solvent, and the system is clearly in the viscous drag regime. The force on the nanoparticle in this regime is essentially constant as a function of separation. The magnitude of the force scales linearly with velocity as hydrodynamic theory predicts in this velocity range. At moderate separation distances, the separation-dependent interaction of the coatings dominates the force. Both coating interactions and hydrodynamic forces play significant roles. The hydrodynamic forces increase with proximity as the solvent is forced from the small space between the nanoparticles. We note that in this region the force is strongly separation- and velocity-dependent. Finally, for very

small separations, the chains of the coating become close-packed and the force increases rapidly. This final region is unlikely to be explored by nanoparticles in solution as the energies associated with these separations are orders of magnitude above the thermal background  $k_B T$  under normal processing conditions.

In conclusion, we have presented results for large-scale simulation of coated nanoparticles in an explicit solvent. We measured the forces on these nanoparticles as a function of separation in two geometries and for several velocities. For separations larger than  $R_{\max}$ , analytical hydrodynamic results for colloidal particles held even at the nanoscale. For two nanoparticles, at large separations the forces were dominated by hydrodynamic forces, specifically viscous drag. For separations less than  $2R_{\max}$ , the interparticle forces were dominated by contact and short-range hydrodynamic forces. In all cases, the functional coating completely suppressed the force oscillations which are observed for uncoated rigid particles of this size in explicit solvents. We observed a similar qualitative response for alkane-coated silica nanoparticles in decane. Results from an extensive series of simulations which investigate the role of chain length, grafting density, and core nanoparticle size will be reported elsewhere.

The authors thank Frank van Swol and Burkhard Dünweg for useful discussions. We thank the New Mexico Computing Application Center (NMCAC) for generous allocation of computer time. This work is supported by the Laboratory Directed Research and Development program at Sandia National Laboratories. Sandia is a multiprogram laboratory operated by Sandia Corporation, a Lockheed Martin Company, for the United States Department of Energy's National Nuclear Security Administration under Contract DE-AC04-94AL85000.

- 
- [1] J. Klein, *Annu. Rev. Mater. Sci.* **26**, 581 (1996).
  - [2] G. S. Grest, *Adv. Polym. Sci.* **138**, 149 (1999).
  - [3] G. H. Fredrickson and P. Pincus, *Langmuir* **7**, 786 (1991).
  - [4] C. N. Likos, *Phys. Reports* **348**, 267 (2001).
  - [5] H. Hasimoto, *J. Fluid Mech.* **5**, 317 (1959).
  - [6] B. Dünweg and K. Kremer, *J. Chem. Phys.* **99**, 6983 (1993).
  - [7] S. Jenkins, S. R. Kirk, M. Persson, J. Carlen, and Z. Abbas, *J. Chem. Phys.* **127**, 224711 (2007); *J. Chem. Phys.* **128**, 164711 (2008).
  - [8] Y. Qin and K. A. Fichthorn, *J. Chem. Phys.* **119**, 9745 (2003); *J. Chem. Phys.* **127**, 144911 (2007).
  - [9] H. Brenner, *Chem. Eng. Sci.* **16**, 242 (1961).
  - [10] M. Vergeles, P. Keblinski, J. Koplik, and J. R. Banavar, *Phys. Rev. E* **53**, 4852 (1996).
  - [11] S. R. Challa and F. van Swol, *Phys. Rev. E* **73**, 016306 (2006).
  - [12] K. A. Fichthorn and Y. Qin, *Ind. Eng. Chem. Res.* **45**, 5477 (2006).
  - [13] H. Kim, D. Bedrov, G. D. Smith, S. Shenogin, and P. Keblinski, *Phys. Rev. B* **72**, 085454 (2005).
  - [14] K. T. Marla and J. C. Meredith, *J. Chem. Theor. Comp.* **2**, 1624 (2006).
  - [15] C. Singh, P. K. Ghorai, M. A. Horsch, A. M. Jackson, R. G. Larson, F. Stellacci, and S. C. Glotzer, *Phys. Rev. Lett.* **99**, 226106 (2007).
  - [16] B. J. Henz, T. Hawa, and M. R. Zachariah, *Langmuir* **24**, 773 (2008).
  - [17] Y. Min, M. Akbulut, K. Kristiansen, Y. Golan, and J. Israelachvili, *Nature Mat.* **7**, 527 (2008).
  - [18] P. Maitra, J. Ding, H. Huang, and S. L. Wunder, *Langmuir* **19**, 8994 (2003).
  - [19] G. D. Smith, O. Borodin, and D. Bedrov, *J. Comp. Chem.* **15**, 1480 (2002).
  - [20] J. S. Smith, O. Borodin, G. D. Smith, and E. M. Kober, *J. Poly. Sci.* **45**, 1599 (2007).
  - [21] W. L. Jorgensen, J. Chandrasekhar, J. D. Madura, R. W. Impey, and M. L. Klein, *J. Chem Phys* **79**, 926 (1983).
  - [22] S. Plimpton, *J. Comp. Phys.* **117**, 1 (1995).
  - [23] R. W. Hockney and J. W. Eastwood, *Computer Simulation Using Particles* (Adam Hilger-IOP, Bristol, 1988).
  - [24] C. D. Lorenz, E. B. Webb III, M. J. Stevens, M. Chandross, and G. S. Grest, *Trib. Lett.* **19**, 93 (2005).
  - [25] P. Bordat and F. Müller-Plathe, *J. Chem. Phys.* **116**, 3362 (2002).
  - [26] D. Bertolini and A. Tani, *Phys. Rev. E* **51**, 1091 (1995).